

# JGR Earth Surface

## RESEARCH ARTICLE

10.1029/2023JF007238

### Key Points:

- The addition of a proxy for marsh sedimentation increases subsidence due to sediment compaction in two laboratory delta experiments
- Subsidence is spatio-temporally variable and dominantly shallow in the experiment with a marsh proxy
- Subsidence rates, even across large areas, are highly variable on short timescales

### Supporting Information:

Supporting Information may be found in the online version of this article.

### Correspondence to:

S. M. Zapp,  
szapp1@lsu.edu

### Citation:

Zapp, S. M., Sanks, K. M., Silvestre, J., Shaw, J. B., Dutt, R., & Straub, K. M. (2023). Sediment compaction in experimental deltas: Toward a meso-scale understanding of coastal subsidence patterns. *Journal of Geophysical Research: Earth Surface*, 128, e2023JF007238. <https://doi.org/10.1029/2023JF007238>






Received 4 MAY 2023  
Accepted 30 OCT 2023

### Author Contributions:

**Conceptualization:** Samuel M. Zapp, Kelly M. Sanks, John B. Shaw, Kyle M. Straub  
**Data curation:** Samuel M. Zapp, Kelly M. Sanks, Jose Silvestre, Ripul Dutt, Kyle M. Straub  
**Formal analysis:** Samuel M. Zapp  
**Funding acquisition:** John B. Shaw, Kyle M. Straub  
**Investigation:** Samuel M. Zapp, Kelly M. Sanks, Jose Silvestre, John B. Shaw, Kyle M. Straub  
**Methodology:** Samuel M. Zapp, Kelly M. Sanks, Jose Silvestre, John B. Shaw, Kyle M. Straub  
**Project Administration:** John B. Shaw, Kyle M. Straub  
**Resources:** John B. Shaw, Kyle M. Straub  
**Software:** Samuel M. Zapp, Kelly M. Sanks, Kyle M. Straub

© 2023. American Geophysical Union.  
All Rights Reserved.

## Sediment Compaction in Experimental Deltas: Toward a Meso-Scale Understanding of Coastal Subsidence Patterns

Samuel M. Zapp<sup>1,2</sup> , Kelly M. Sanks<sup>1,3</sup> , Jose Silvestre<sup>3</sup> , John B. Shaw<sup>1</sup> , Ripul Dutt<sup>3</sup>, and Kyle M. Straub<sup>3</sup> 

<sup>1</sup>Department of Geosciences, University of Arkansas, Fayetteville, AR, USA, <sup>2</sup>Department of Oceanography and Coastal Science, Louisiana State University, Baton Rouge, LA, USA, <sup>3</sup>Department of Earth and Environmental Sciences, Tulane University, New Orleans, LA, USA

**Abstract** We present the first investigation of subsidence due to sediment compaction and consolidation in two laboratory-scale river delta experiments. Spatial and temporal trends in subsidence rates in the experimental setting may elucidate behavior which cannot be directly observed at sufficiently long timescales, except for in reduced scale models such as the ones studied. We compare subsidence between a control experiment using steady boundary conditions, and an otherwise identical experiment which has been treated with a proxy for highly compressible marsh deposits. Both experiments have non-negligible compactional subsidence rates across the delta-top, comparable in magnitude to our boundary condition relative sea level rise rate of 250  $\mu\text{m/hr}$ . Subsidence in the control experiment (on average 54  $\mu\text{m/hr}$ ) is concentrated in the lowest elevation (<10 mm above sea level) areas near the coast and is likely related to creep induced by a rising water table near the shoreface. The treatment experiment exhibits larger (on average 126  $\mu\text{m/hr}$ ) and more spatially variable subsidence rates controlled mostly by compaction of recent marsh deposits within one channel depth ( $\sim$ 10 mm) of the sediment surface. These rates compare favorably with field and modeling based subsidence measurements both in relative magnitude and location. We find that subsidence “hot spots” may be relatively ephemeral on longer timescales, but average subsidence across the entire delta can be variable even at our shortest measurement window. This suggests that subsidence rates over a short time frame may exceed thresholds for marsh platform drowning, even if the long term trend does not.

**Plain Language Summary** Coastal and deltaic wetlands sit very near sea level. They accumulate a compressible mixture of organic material and mud which is deposited by tides and/or overbank flooding from rivers. As a result, these wetland environments can rapidly build elevation to keep pace with a significant amount of relative sea level rise. Over time, more sediment is delivered on top of the initially porous surface layers and they become compacted as they are buried, contributing to a downward movement of the land surface known as subsidence. Subsidence is a hazard that threatens infrastructure and worsens coastal flooding. Here we examine the spatial and temporal patterns of subsidence in a small (about 2 m<sup>2</sup>) physical delta experiment which includes a compressible proxy for wetland sediments. We find that subsidence is significantly higher where these wetland sediments have recently been deposited and driven by their compaction in the very shallow subsurface.

## 1. Introduction

Subsidence, the downward directed movement of the Earth surface, exerts a fundamental physical control on river deltas. Summed with changes in eustatic sea level, subsidence increases relative sea level rise (RSLR) which controls the equilibrium size of a delta, and the dynamics of its channels and marshes (Liang et al., 2016; Moodie & Passalacqua, 2021; Morton et al., 2006). Sediment deficits and projections of future sustainability of deltas often include subsidence as one of the largest uncertainties (Sanks et al., 2020; Shirzaei et al., 2021). Hence, subsidence affects these dynamic ecosystems and several hundred million people that live on river deltas.

The stability of coastal wetlands is closely coupled to subsidence because they exist within the intertidal zone and accrete as a function of elevation relative to sea level (Cahoon et al., 2019; Morris et al., 2002). These threatened environments provide valuable ecosystem services including storm surge protection, carbon sequestration, and water quality regulation (Engle, 2011). Wetland retreat is expected to respond non-linearly with future RSLR projections (Kirwan & Guntenspergen, 2010; Mariotti, 2020). In South Louisiana alone, over 5,000 km<sup>2</sup>

**Supervision:** John B. Shaw, Kyle M. Straub  
**Validation:** Samuel M. Zapp, John B. Shaw  
**Visualization:** Samuel M. Zapp  
**Writing – original draft:** Samuel M. Zapp  
**Writing – review & editing:** Samuel M. Zapp, Kelly M. Sanks, Jose Silvestre, John B. Shaw, Ripul Dutt, Kyle M. Straub

of coastal wetlands have been lost since 1930 (Couvillion et al., 2017), largely due to high, spatio-temporally variable subsidence rates from the compaction of highly compressible marsh deposits in the shallow subsurface (Nienhuis et al., 2017; Törnqvist et al., 2008). On modern river deltas, subsidence within the top several meters of stratum, often including a significant amount of organic material, can dominate background RSLR (eustatic sea level rise plus tectonic regional subsidence) over large areas by as much as an order of magnitude, at least on short timescales (Erban et al., 2014; Jankowski et al., 2017; Zumberge et al., 2022).

Measured subsidence rates on river deltas worldwide are both highly spatially and temporally variable. While subsidence rates over annual to decadal timescales can approach, and even exceed, a centimeter per year on the Mississippi (Nienhuis et al., 2017), Mekong (Erban et al., 2014; Minderhoud et al., 2017) and Ganges-Brahmaputra (Steckler et al., 2022) Deltas, there is disagreement about the upper bound of annual subsidence rates and whether or not subsidence maxima correlate with geologic controls such as Holocene deposit thickness (Byrnes et al., 2019; Jankowski et al., 2017). Millennial scale subsidence rates are consistently estimated to be significantly lower (Chamberlain et al., 2021; Kooi & de Vries, 1998; Meckel et al., 2006; Törnqvist et al., 2008; van Asselen, 2011). It remains unclear if areas of high subsidence can persist on century and longer timescales due to a lack of direct measurement going back further than about 15 years. Additionally, the overprinting of several possible subsidence mechanisms including sediment compaction, faulting, anthropogenic soil drainage, and deep fluid withdrawal make it difficult to understand which processes are driving the complexity of observed subsidence rates (Chang et al., 2014; Dokka, 2006; Yuill et al., 2009). Understanding the degree to which natural processes and human activity each impact different subsidence mechanisms is crucial to proposed land loss mitigation plans such as sediment diversions and wetland restoration, which are planned on decadal to centennial timescales.

Our understanding of the co-evolution between delta morphodynamics, marsh growth, and coincident subsidence remains relatively limited. This incomplete understanding can be attributed to our inability to directly observe the processes of delta evolution (i.e., aggradation, channel incision, avulsion) and marsh platform growth over sufficiently long “meso-timescales” ( $10^2$ – $10^5$  years), as well as difficulty isolating the various forcing conditions that drive morphodynamic change and mechanisms that contribute to coastal subsidence (Hoyal & Sheets, 2009; Yuill et al., 2009).

Here we describe the autogenic subsidence behavior of two laboratory scale delta experiments, one treated with a proxy for marsh deposits (TDWB-19-2, hereafter called the treatment experiment) and one untreated experiment (TDB-18-1, hereafter called the control experiment), in order to better understand how the coupling between deltas and marshes impacts the spatio-temporal variability of subsidence rates throughout delta evolution. Reduced-scale experiments are effective at creating analogous kinematics and spatial architecture to autogenic behavior observed in field deltas (Paola et al., 2009). They are a particularly useful tool to understand “meso-scale” delta evolution that cannot be fully captured by continuous field measurement during active morphodynamic changes, nor reconstructed by stratigraphic interpretation (Paola et al., 2009). Our setup is designed to dissociate background RSLR applied as a boundary condition ( $RSLR_b$ ; meant to represent both tectonic subsidence and eustatic sea level rise) from spatially and temporally variable subsidence ( $\sigma_s$ ) that emerges within the experiment.

This study is part of a larger project (including Sanks et al. (2022a)) which aims to assess the impact of marshes on a wide range of deltaic processes, from delta-top kinematics to stratigraphic patterns. No studies have previously described autogenic subsidence due to sediment compaction (hereafter, just subsidence) in a delta experiment. We hypothesize that the addition of the marsh proxy in the treatment experiment will generate significant subsidence across the portion of the delta that regularly receives marsh deposits. In this case, subsidence rates will likely be correlated with underlying marsh deposit thickness. If subsidence rates are sufficiently large over long enough timescales, they could influence a wide range of geomorphic processes including marsh drowning, channel kinematics (Liang et al., 2016; Moodie & Passalacqua, 2021), and delta progradation (Chamberlain et al., 2021).

## 2. Methods

### 2.1. Experimental Setup

We analyze two delta experiments conducted at the Tulane Sediment Dynamics and Stratigraphy Lab. The experiments have identical boundary conditions, and approached a dynamic equilibrium state under constant forcing

**Table 1**  
*Boundary Conditions of Both Experiments*

Delta experiment	Experiment run time (hr)	$Q_w$ (m <sup>3</sup> /s)	$Q_s$ (kg/h)	$RSLR_b$ (mm/h)	Sediment mixture
Control TDB-18-1)	560	$1.72 \times 10^{-4}$	1.40	0.25	Strongly cohesive mixture (Straub et al., 2015)
Marsh (TDWB-19-2)	560	$1.72 \times 10^{-4}$	1.40	0.25	Strongly cohesive mixture (Straub et al., 2015); EPK marsh proxy ( $\approx 200$ g/2 hr)

conditions of sea level rise rate ( $RSLR_b$ ), basin geometry (2.8 m across with an open seaward boundary), and water ( $Q_w$ ) and sediment discharge ( $Q_s$ ) listed in Table 1. Each experiment was allowed to prograde for 120 hr before hour zero of run time. The treatment experiment differed only in that a proxy for marsh sedimentation was applied to regions near sea level (−9 to 5 mm relative to sea level, hereafter RSL), resulting in about 8% of the final deposit mass and 15% of the final deposit volume (Sanks et al., 2022a). Therefore, significant statistical differences in subsidence rates can be attributed to the impact of the marsh proxy deposits.

Topography was measured with a Lidar scanner to create digital elevation models (DEMs) with a  $5 \times 5$  mm plan-form grid, and a sub-mm vertical resolution (Supporting Information S1). In the control experiment, scans were collected at the beginning of each run hour. In the treatment, scans were collected at the beginning of every even run hour directly before the marsh proxy was dispensed, as well as 48 min into each run hour. Changes in elevation through time with respect to the stationary Lidar scanner are attributable to sediment deposition, erosion, and/or subsidence ( $\sigma_s$ ).  $RSLR_b$  is generated by gradually raising the water level in the basin rather than lowering the basin itself, so base level changes are not captured in Lidar measurements. Screening out areas of fluvial sediment deposition and erosion (e.g., locations with surface water present, including subaqueous areas) allows for measurement of subsidence ( $\sigma_s$ ) at the two-hour timescale in both experiments, as well as the initial thickness of each marsh deposit in the treatment experiment. This procedure is described in Section 2.2.

The marsh proxy was distributed based on a simple conceptual model relating primary production in salt marshes to elevation relative to sea level (Morris et al., 2002). As such, the distribution patterns here are primarily intended to mimic marshes present in coastal settings, but may also represent tidal mud flats or other coastal areas that accumulate fine-grained sediment as a function of elevation relative to sea level. Every 2 hr, a DEM was averaged at the 0.015 m<sup>2</sup> scale on a hexagonal grid in order to identify suitable elevations for marsh deposition (Figure 1a). The marsh proxy (Edgar Plastic Kaolin, or EPK) was distributed to each hexagon each distribution cycle (every 2 hr) as a function of this averaged elevation (mm) RSL at that time step. All binned locations with an average elevation between −9 and 5 mm RSL (hereafter referred to as the “marsh window”) at a given time received marsh sediment from a vibrating sieve (Figure 1a). On average, 200 g of marsh proxy were deposited during each distribution cycle, but the amount varied due to the number of hexagons within the marsh window at a given time, and to a lesser extent, mechanical imprecision in distributing the prescribed deposit thickness (Figure 1b; Sanks et al., 2022a). The order in which distribution hexagons were queried was alternated from basin left to basin right in order to mitigate spatial biases over timescales longer than a single distribution cycle.

The proxy's porosity when settling through water was measured in pre-experiment trials to be  $\geq 90\%$  when first deposited. This gives it significantly more compaction potential than the fluvially introduced clastic sediment which had approximately 75% initial porosity. The sediment mixture delivered by river transport to both experiments ranges in grain size from coarse sand to clay and contains a polymer to increase sediment cohesion. It has been described in Straub et al. (2015).

This setup was not meant to imitate any particular field setting, but designed to create a steady-state scenario where the unstable (−9 to −5 mm RSL) and stable (0–5 mm RSL) marshes would inevitably lose elevation in the absence of mineral sediment nourishment, while maximally productive (−5 to 0 mm RSL; Figure 1b) areas would outpace  $RSLR_b$ , at least over short timescales. Similarly to the Morris et al. (2002) model, the highest (i.e., “stable”) and lowest (i.e., “unstable”) elevation marshes accrete slower than optimal elevation marshes (i.e., “maximum production”) which fall in between. Tides are not physically present in this experiment, so accretion rates are schematized as a function of elevation RSL rather than operating as a function of their position in the tidal frame, as Morris et al. (2002) described. Sediment accretion (both through marsh proxy deposition and fluvial transport), erosion,  $RSLR_b$ , and  $\sigma_s$  combine to dynamically alter delta morphology through time and allow each location to move in, out, and across the marsh window. Locations sitting between −9 and −5 mm RSL

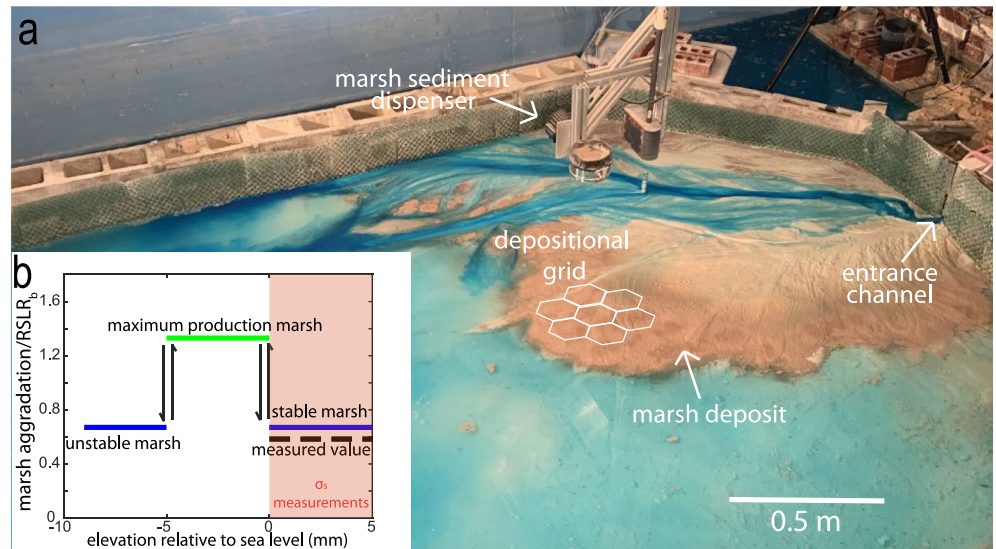


**Figure 1.** (a) An image of the treatment experiment during a marsh distribution cycle. The metal apparatus is a sieve mounted to a low-frequency vibrator which shakes out marsh proxy. The darker brown sediment is exposed marsh deposits. White hexagons represent the grid pattern that marsh proxy was distributed over. (b) Elevation based rules for marsh deposition rates. Mean values of marsh deposition relative to  $RSLR_b$  for each zone are depicted as horizontal blue and green lines. The dashed black line represents Lidar measured values of initial marsh thickness for subaerial deposits (see Section 2.2). Deposition occurs every 2 hr of run time during the treatment experiment. The maximum production marsh region ( $-5$  to  $0$  mm RSL) aggrades faster than  $RSLR_b$ , while unstable (well below sea level) and stable (above sea level) regions aggrade slower than  $RSLR_b$ . Subsidence measurements were collected in subaerial locations via repeated Lidar measurements.

and  $0$ – $5$  mm RSL accreted marsh proxy at  $0.67$  times  $RSLR_b$  on average, and locations in the  $-5$  to  $0$  mm RSL elevation range accreted marsh proxy at  $1.33$  times  $RSLR_b$ , based on measurements of flux through the marsh sediment dispenser (Figure 1b). An overall mean surficial marsh deposit thickness for the “stable” marsh was collected via repeat Lidar scans (see Section 2.2), showing a comparable but slightly lower aggradation rate of  $0.58$  times  $RSLR_b$  (dashed line in Figure 1b) compared to the accretion rate estimated via sediment flux through the marsh dispenser ( $0.67$  times  $RSLR_b$ ). These accretion rates are simply meant to create a situation where maximally productive marshes generally maintain their elevation in response to RSLR, while marshes at the higher and lower extremes of the elevation window they can habitate do not. This situation would arise in a real world setting where a marsh platform is roughly in equilibrium with RSLR and neither systematically drowning nor prograding.

## 2.2. Subsidence and Marsh Thickness Maps

Subsidence maps for both experiments were generated by differencing DEMs and screening out areas that were flooded by sea level or that received surface water flow at some point during the time step. This was done to remove all sediment transport processes and isolate subsidence in “quiescent” areas. Areas covered by surface water were removed by a color threshold screen. Differenced DEM values lower than  $-1,000$   $\mu\text{m}$  or greater than  $5,000$   $\mu\text{m}$  were considered erroneous and removed from the data set.

Control experiment DEMs were differenced by appropriately screening each scan, subtracting the previous scan from a given scan, and then summing the resulting two-hour DEMs of difference. The treatment experiment DEMs were differenced by subtracting a scan collected 48 min into each 2-hr time step from each scan collected every even hour of experimental run time (72 min later). This was done to exclude marsh accretion in the first 48 min of each two-hour period of run time. The resulting subsidence maps were then multiplied by a correction factor of  $120/72$  to account for “lost” time and make them equivalent to two-hour DEMs of difference. Therefore, subsidence rates can be compared between the experiments at a two-hour temporal resolution. The linear correction factor applied to the treatment experiment measurements may be conservative given that the highest rates of compaction occur shortly after deposition. However, the estimate of initial marsh proxy porosity (90%) was



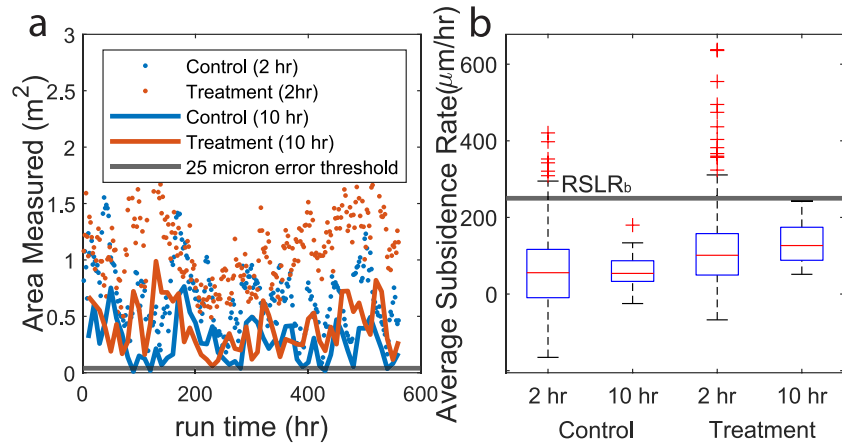


**Figure 2.** (a) Time series of the delta area where Lidar-based subsidence measurements were possible. Note that the number of measurements for the treatment was sufficiently large that error was always less than 25  $\mu\text{m}$ , and generally less than 10  $\mu\text{m}$ . (b) Distributions of spatially averaged subsidence rate for each 2 and 10-hr time step for both experiments. Boxplots span the 25th to 75th percentile values, and whiskers extend up to 1.5 times the interquartile range. These subsidence rates are generally greater in the treatment experiment than the control.

taken from samples allowed to settle for a similar amount of time, so calculations involving this assumption (e.g., Figure 7) are consistent with Lidar based measurements. Subsidence rates were also compared at ten-hour time steps by summing consecutive two-hour subsidence maps and excluding points which did not return a value each time step. Analyses of subsidence rates in “low elevation areas” of the delta top were also conducted by restricting the subsidence maps to locations between 0 and 15 mm RSL (Figure 3). See Supporting Information S1 for more details on the procedures described above and SI materials for videos of subsidence maps through time.

An initial thickness map of each surficial marsh deposit was separately quantified by differencing the scan taken right after distribution (48 min into an hour) and the scan taken right before, then screening out areas outside of the marsh window. Areas receiving surface water were excluded in the same manner as in the subsidence maps.

Marsh maps derived from Lidar scans were stacked to create a “synthetic stratigraphy” representing the total uncompacted thickness of the marsh maps at each location. The marsh maps do not account for submarine marsh deposition, so they do not equate to total initial marsh deposit thickness, only the thickness of subaerially deposited marsh. However, this marsh thickness can be normalized by the thickness of the final deposit to yield a synthetic marsh fraction which is comparable to the directly measured marsh thickness from stratigraphy.

### 2.3. Measurements of Marsh Seams in Stratigraphy

At the end of the treatment experiment, the delta was sectioned along strike parallel to the entrance channel at 10 cm intervals. The thicknesses of buried marsh seams were measured at a several geographic locations with varying burial depths ( $n = 8$ ). Each data point is displayed in Figure 7a. Measurements of porosity (used to calculate void ratio) were taken from individual seams of preserved marsh proxy at various ultimate burial depths (Figure 7a). This was done by taking cores, freezing them, cutting out marsh seams of known thicknesses, and then weighing the seams to produce a bulk density which could be converted to porosity ( $n$ ) and then void ratio ( $e$ ) by the equation  $e = n/(1 - n)$ . The cumulative marsh thickness at each location was divided by the entire deltaic deposit thickness to get the marsh fraction in stratigraphy.

This experimental proxy for compressible marsh sediments compacted to less than 25% of its initial thickness under the minor loading (<1 kPa) experienced in the experiment. While this mimics the compaction found in real deltas, the exhaustion of primary consolidation potential observed within Holocene strata (Keogh, 2020; Keucher, 1994) was not achieved. Additionally, organic-rich field samples experience a high degree of secondary compression due to the collapse of peat particles (Mesri et al., 1997), as well as volumetric losses from oxidation (Chambers et al., 2019). Our marsh proxy is entirely mineral sediment. Even so, the autogenic compaction patterns produced sediment compaction over thicknesses less than a channel depth, providing a compelling comparison to the field.

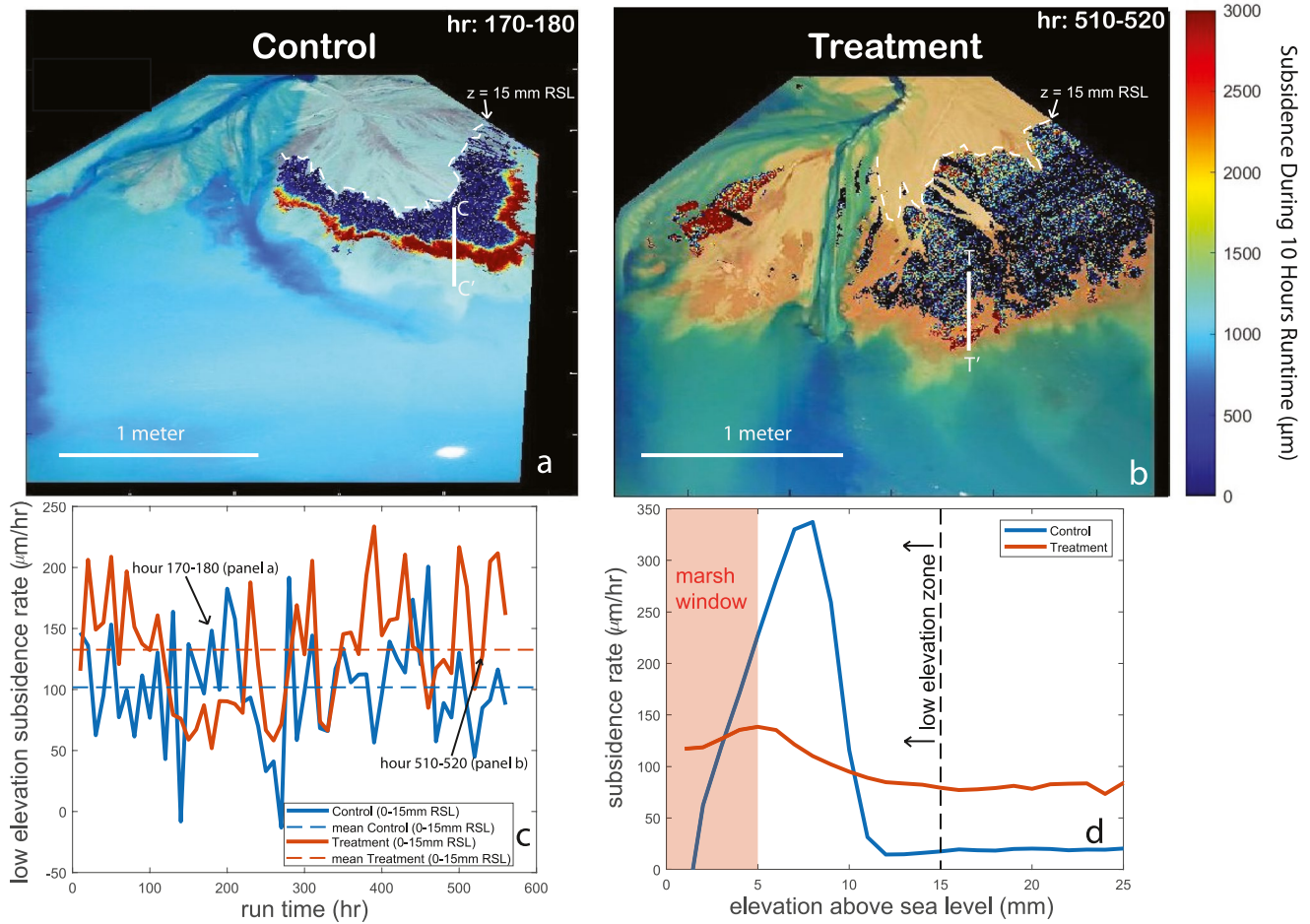


**Figure 3.** (a) Overhead image of control experiment at hour 180 overlain with subsidence map (5 mm × 5 mm resolution) of the previous 10 hr. Dashed white line here and in panel b represents 15 mm elevation RSL contour, or the top of the “low elevation zone.” (b) Overhead image of treatment experiment at hour 520 overlain with subsidence map of the previous 10 hr. (c) Time series of average subsidence rates in the low elevation zone (spanning 0–15 mm RSL) for each 10-hr time step for both experiments. Subsidence rates are variable through time, but do not exhibit a temporal trend. Mean subsidence rates in the 0–15 mm RSL region for the control and treatment are marked by dashed lines. The time steps displayed in panels (a) and (b) are marked. (d) Time averaged profiles of subsidence as a function of elevation above relative sea level for both experiments. The window of active marsh deposition for the treatment experiment is shaded orange, and the upper boundary of the low elevation zone is delineated by a dashed black line.

### 3. Results

#### 3.1. Overall Subsidence Trends

Both experiments exhibit measurable subsidence in unchannelized subaerial portions of the delta over timescales of 2 and 10 hr. The quiescent region of measurement varied with delta top channel dynamics, but averaged  $0.27$  and  $0.40 \text{ m}^2$  on the 10 hr timescale for the control and treatment respectively, resulting in uncertainties less than  $25 \text{ } \mu\text{m}$  for each experiment (Figure 2a, Supporting Information S1). Both experiments also exhibit significant spatial and temporal variability. However, the treatment experiment has a significantly higher delta-wide mean subsidence rate of  $126 \pm 108 \text{ } \mu\text{m/hr}$  compared to  $54 \pm 103 \text{ } \mu\text{m/hr}$  for the control experiment (over 10 hr; Figure 2b). A paired-sample *t*-test indicates that delta-wide subsidence rates are statistically distinct between the two experiments at both the two-hour and ten-hour timescales ( $p < 0.01$ ).

Subsidence rates in low elevation areas of the delta top (0–15 mm RSL) do not show a significant temporal trend over either experiment (Figure 3c), but regularly fluctuate by more than  $100 \text{ } \mu\text{m/hr}$  across the delta top. The deposit aggrades from 25 to 165 mm thick at the shoreline throughout the experiment, so the lack of a gradual increase in rates demonstrates that subsidence is uncorrelated with total deposit thickness. Average subsidence rates rarely approach imposed RSLR ( $RSLR_b = 250 \text{ } \mu\text{m/hr}$ ) for the treatment and never do in the control when

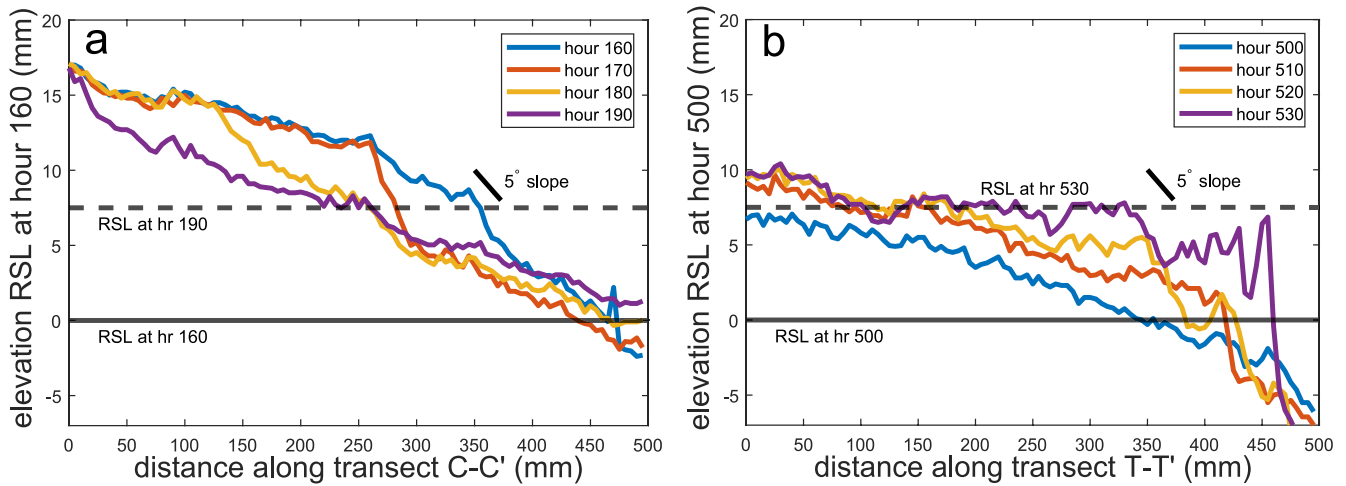


**Figure 4.** (a) Profile of the control experiment topography along transect C-C' from Figure 3a at hours 160, 170, 180, and 190. Significant bed lowering occurs above sea level and landward of a subaerial slope break. (b) Profile of the treatment topography along transect T-T' from Figure 3b at hours 500, 510, 520, and 530. No subaerial slope break is present here. The profile is net aggradational everywhere over this time period in spite of subsidence because of marsh deposition (especially from 200 to 350 mm along transect).

averaged over 10-hr periods. Therefore, most of the total RSLR is created by imposed rising base level, as opposed to compactional subsidence in both cases.

Subsidence varies in both experiments as a function of elevation relative to sea level. Subsidence is highly concentrated near the coastline in the control experiment, but more dispersed throughout the subaerial delta and highly spatially variable on short timescales in the treatment experiment (Figures 3a and 3b). Subsidence in the control is clearly related to elevation above sea level (Figure 3d). Subsidence rates peak at 7–8 mm above sea level and become minimal at around 10 mm above sea level. This subsidence peak moves with the shoreline through transgressions and regressions. It is associated with a slope maximum (Figure 4a), which consistently occurs 5–10 mm above sea level and backsteps as base level rises. In contrast, the treatment experiment subsidence rates are relatively consistent. Subsidence rates are slightly higher in the window of active marsh deposition, as well as slightly above it in areas that had often recently been in the marsh window. Subsidence rates only decrease by 20%–40% in the 20 mm above the marsh window. The subaerial slope break observed in the control (Figure 4a) is notably absent in the treatment (Figure 4b), where slopes on the order of several degrees only occur below sea level.

### 3.2. Treatment Experiment Subsidence Pattern and Mechanism

The spatiotemporal subsidence patterns in the treatment experiment are more complex than in the control. We study the persistence of subsidence across the delta over a 2-hr timescale. Correlations are drawn by gridding each subsidence map into 50 mm × 50 mm blocks, averaging values within every block, and plotting the subsidence rate at each block against either the subsidence rate at each block 2 hr later or the immediately preceding surficial marsh deposit thickness at each block. Subsidence rates are highly transient through time at the 2-hr scale, with subsidence rarely showing significant correlation ( $R > 0.5$ ) over subsequent maps ( $n = 280$ ; orange histogram in Figure 5). This means that subsidence “hot spots” rarely persist through repeated measurements at the same location.

Spatially distributed subsidence rates correlate somewhat better with the thickness of the most recent marsh deposit (blue histogram in Figure 5), with correlations ( $R$ ) typically ranging from 0.3 to 0.6 for a 2-hr time step. This marginal correlation declines when comparing 2-hr subsidence to deposition rates averaged over four or 6 hr (not shown). Consequently, short-term subsidence rates are somewhat higher where recent marsh deposits are thicker.

Despite limited short timescale predictability, there is a better correlation between marsh presence and subsidence evaluated over the entire experiment. The fraction of the total stratigraphic package comprised of marsh

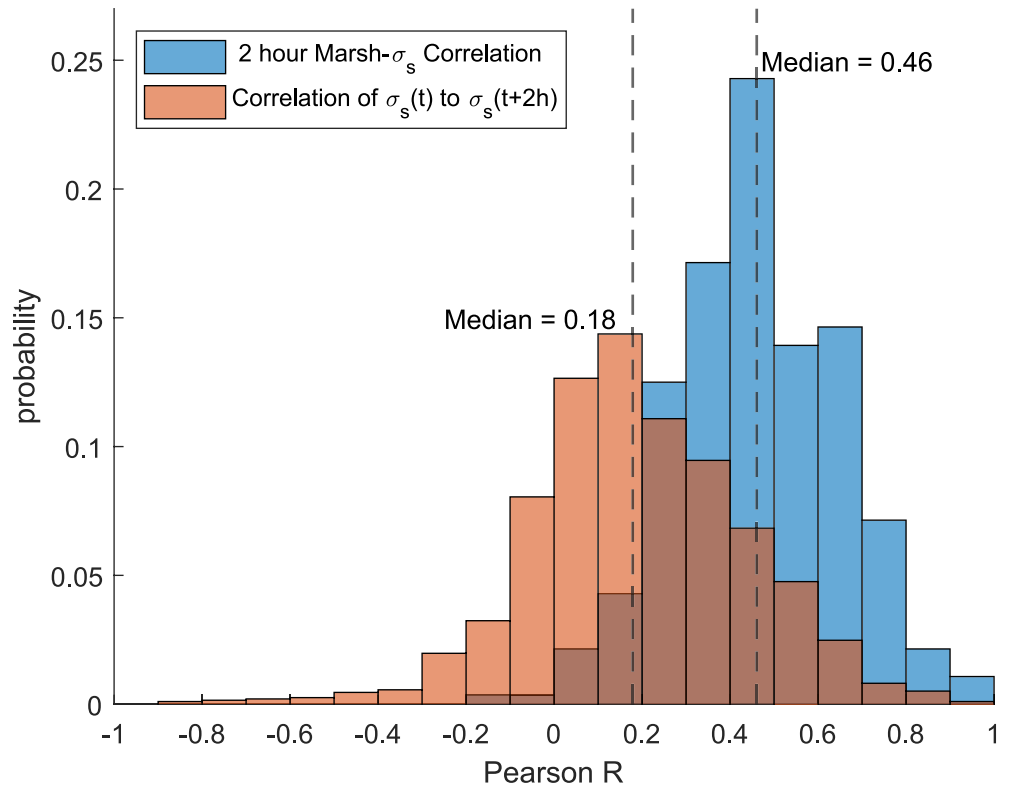


**Figure 5.** Histograms showing the distribution of correlation coefficients (Pearson  $R$ ) between all local subsidence rates from one time step to the next (in orange), and between all local subsidence and the most recent marsh deposit thickness (in blue) in the treatment experiment. Median Pearson  $R$  values for both histograms are also shown.

deposits is measured both directly (Section 2.3), and by summing all individual surficial marsh deposit thicknesses. Though the summed marsh map approach excludes marsh deposited below sea level, and thus underestimates marsh fraction, the two methods follow a similar trend (Figure 6b). Both methods also correlate well with average subsidence rates throughout the experiment as a function of distance downstream of the entrance channel pictured in Figure 1a (Figure 6a). Each measurement type peaks around the average shoreline position, which is located about 1,100 mm from the entrance channel (Figure 6a; Sanks et al., 2022a). In other words, long-term subsidence rates are higher where marsh deposits are thicker.

Stratigraphic measurements of porosity (transformed to void ratio,  $e$ ) collected from marsh stratigraphy are used to constrain the vertical profile of subsidence due to marsh compaction. The void ratio of marsh seams decreases with burial depth ( $z$ ; in mm). It is well fit by an exponential decay function  $e(z) = 13.21^{-1.54z}$  with an  $R^2$  of 0.76 (Figure 7a). Under conservation of mass and assuming a constant marsh aggradation rate equal to  $RSLR_b$ , the compaction rate  $s$  at any  $z$  is  $s = RSLR_b * de/dz$ , and the total subsidence at any elevation is  $s$  integrated from maximum depth (here 170 mm) to depth  $z$ :

$$\sigma_s(z) = \int_{\max(z)}^z s dz. \quad (1)$$

Subsidence rates calculated in this way assume a steady input of uncompacted marsh (90% porosity) every 2 hr. Marsh aggradation is estimated to be equal to  $RSLR_b$  (which is the average of stable/unstable and maximum production values) to represent a long-term value for a given seam which likely passed through different productivity bins and may have experienced some reworking before its ultimate preservation. If the likelihood of marsh deposition is assumed to be unchanging through time, areas that received marsh 50% of the time would have 50% of the calculated subsidence rate in this steady-state compaction model. Compaction of fluvial sediment is neglected in this calculation.

The majority of the subsidence in the treatment experiment is associated with the compaction of marsh deposits within 20 mm of the surface, and nearly half occurs above one typical channel depth (Figure 7b). Surface subsidence rates in the compaction model agree well with 10-hr Lidar measurements of surface subsidence clipped to areas actively



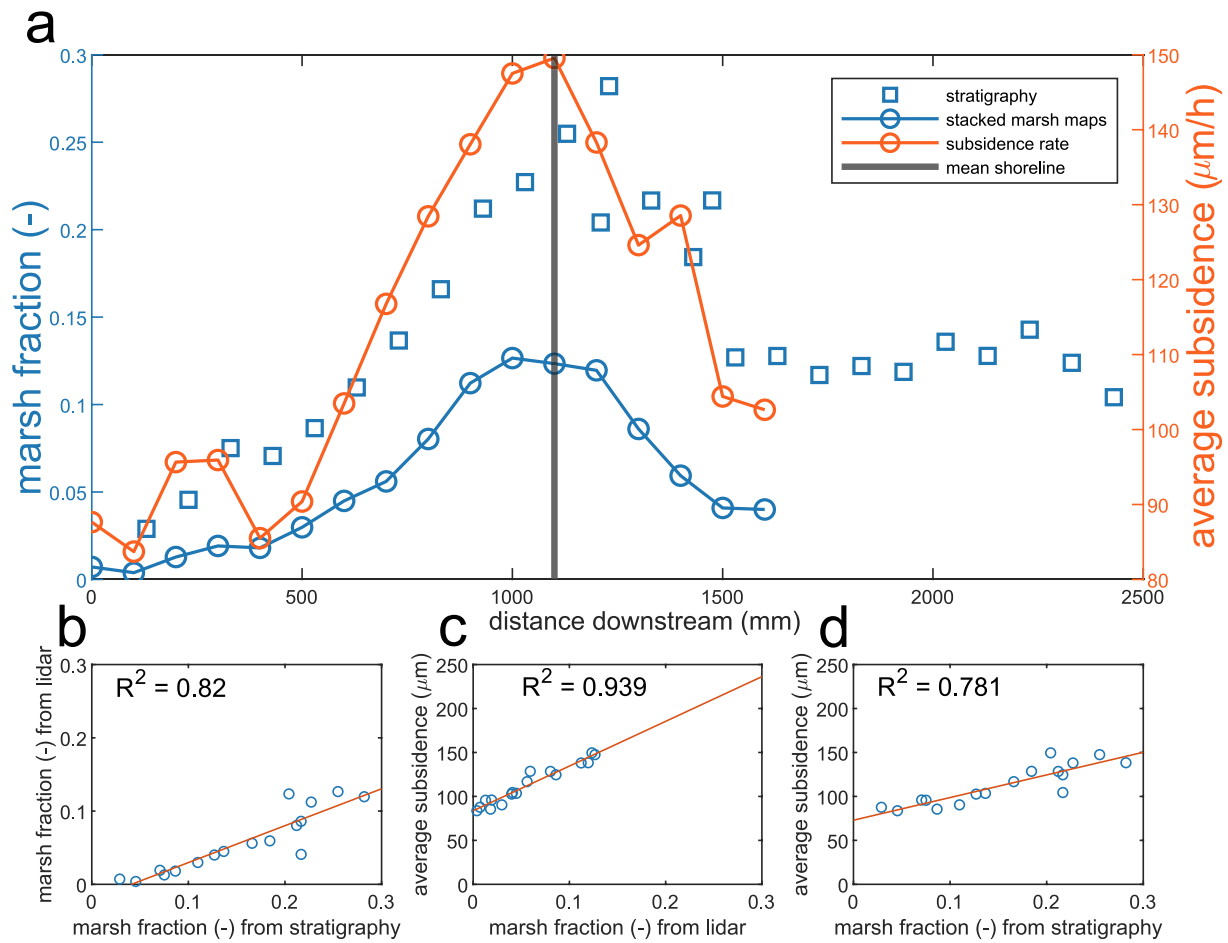


**Figure 6.** Subsidence rate, marsh fraction from stacked marsh maps, and marsh fraction measured from stratigraphy are compared as a function of distance downstream from the entrance channel. (a) Each parameter peaks around the average shoreline position of 1,100 mm downstream of the entrance channel. (b–d) Pair-wise correlation between the three measurement types in (a).

receiving marsh deposition. Agreement is particularly good when the compaction model assumes marsh deposition comprises 25%–50% of aggradation with the remainder being fluvial sediments. Much of the delta is comprised of 15%–30% marsh deposits (Figure 6a; Sanks et al., 2022a). The somewhat higher values from Lidar measurements (mean rate of 126  $\mu\text{m}/\text{hr}$ ) compared to the marsh compaction model assuming 25% marsh deposition (81  $\mu\text{m}/\text{hr}$  at the sediment surface) is likely due to fluvial sediment compaction. These two independent measurement techniques yield a consistent picture of shallow subsidence in the treatment experiment.

#### 4. Discussion

The experimental results presented in this paper suggest that the spatial and temporal structure of shallow subsidence rates are strongly influenced by the presence of compressible marsh deposits in low elevation areas of river deltas. The control experiment exhibited a tight band of subsidence just above sea level. Subsidence patterns in the treatment experiment are widely dispersed and temporally unpredictable at short timescales, but they are somewhat locally controlled by the thickness of the most recent marsh deposit. Over longer timescales, subsidence rates are well predicted by the presence of marsh deposits. Scaling subsidence rates by background RSLR over the duration of the experiment ( $\sigma_j / RSLR_b$ ), we see that the control experiment is 0.2, the treatment experiment is 0.5, and some modern field measurements range between 0.95 and 3.8 (Table 2). Experimental values may be smaller than field values because the marsh proxy is likely less compressible than real world deposits for the reasons described in Section 2.3. Nevertheless, the experimental treatment increased compactional subsidence to be on the same order as measurements from some field-scale deltas, and can similarly exceed  $RSLR_b$  on shorter timescales (Figure 2b).

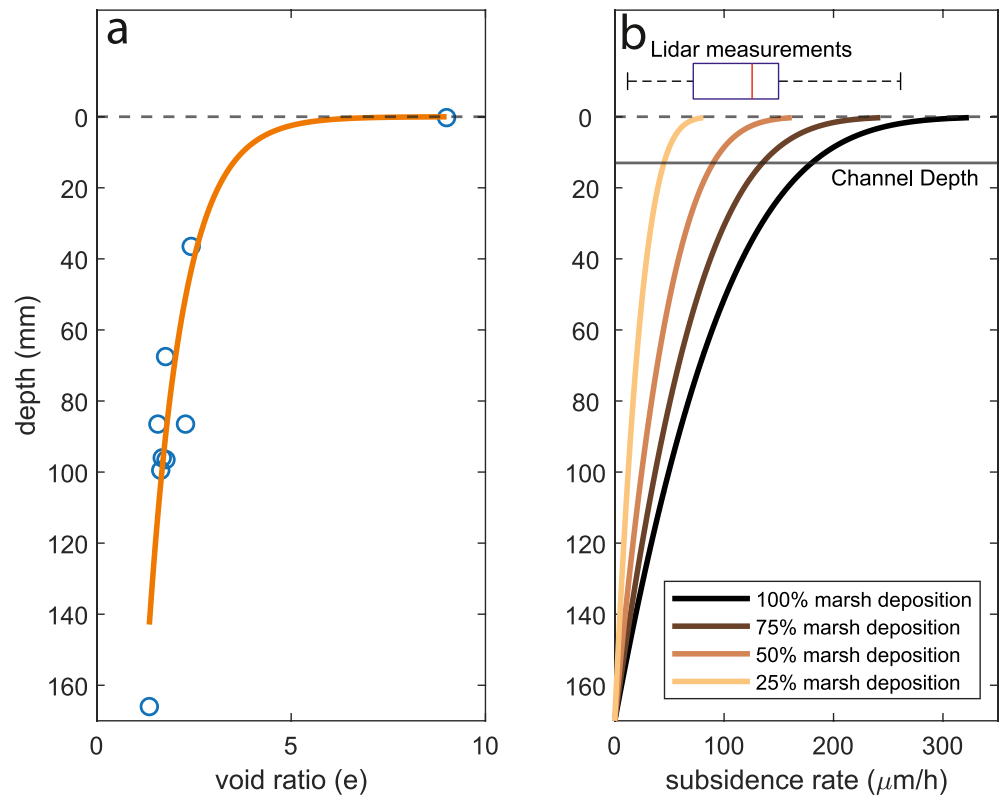


**Figure 7.** Subsidence within marsh deposits calculated from measurements of void ratio within the final deposit. (a) Void ratio as a function of depth. Circles indicate measurements, with exponential fit (see Section 2.3). (b) Subsidence rate with depth for marsh deposits calculated from Equation 1. 100% marsh deposition represents a scenario where marsh is always deposited equal to  $RSLR_b$  and never eroded. Spatially averaged, 10-hr subsidence rates from Lidar measurements for all areas within the marsh window and average channel depth in the treatment experiment are also shown.

**Table 2**  
*Relative Importance of Compactional Subsidence ( $\sigma_s$ ) Versus Background Relative Sea Level Rise ( $RSLR_b$ ) for Field Scale, Experimental, and Modeled River Deltas at a Range of Timescales*

Delta	$\sigma_s$ (mm/yr) (* $\mu$ m/hr)	$RSLR_b$ (mm/yr) (* $\mu$ m/hr)	$\sigma_s/RSLR_b$ (-)	Timescale of measurement, $t_{meas}$ (yr), (*hr)	Compensation timescale, $t_{comp}$ (yr), (*hr)
Control (TDB-18)	*54	*250	0.22	*2–10	*58.4
Treatment (TDWB-19-2)	*126	*250	0.50	*2–10	*53.6
Modern Mississippi	7.1	4.3	1.66	10	$\sim 10^5$
Modern Mekong	16	4.2	3.81	$\sim 10$	$\sim 3 \times 10^4$
Modern Po	4	4.2	0.95	$\sim 10$	$\sim 2 \times 10^4$
Holocene Mississippi	1–5	$\sim 1.5$	0.67–3.33	$\sim 10^3$	$\sim 10^5$
Hydrodynamic Model	0.1–1	$\sim 1$	0.1–1	$\sim 5 \times 10^4$	$\sim 10^5$

*Note.* Rates for Mississippi (Nienhuis et al., 2017), Po (Bruno et al., 2017; Syvetski et al., 2009), and Mekong (Erban et al., 2014; Ishii et al., 2021) are based on modern measurements. Millennial scale rates for the Mississippi (Törnqvist et al., 2008) and longer timescale rates from a hydrodynamic compaction model (Kooi & de Vries, 1998) are included to compare subsidence measurements at different timescales.  $RSLR_b$  were estimated for field deltas by adding 1 mm/yr of deep-seated subsidence to eustatic sea level rise rates. The compensation timescale is defined as the mean channel depth divided by the long term aggradation rate (or  $RSLR_b$  in the experiments).

We did not anticipate any subsidence in the control experiment, yet it revealed a well-organized signature. We interpret the apparent subsidence in the control experiment to be at least partially due to soil creep, slumping, or mudflows near sea level. Mudflows can be triggered due to a rising water table in clay rich soils (such as the overbank fraction of the fluvial sediment mixture) at comparable slopes to those seen at the shoreline of the control experiment (5°; Vallejo, 1980). The water table rises with  $RSLR_b$ , so mudflow is deemed the most likely mechanism triggering the “subsidence” band. This localized phenomenon may be semi-continuous or punctuated but occurring more frequently than the two-hour timescale of subsidence map collection. As such, it is effectively a kind of soil creep at this scale. The relative contributions of vertical compaction (which would classically be included as a subsidence mechanism) and lateral creep/mudflow (which may not be strictly classified as subsidence) to this feature remain unquantified. Local downslope bed level increases are smaller than the volume of sediment removed (Figure 4a), so compaction must be a significant component. For this reason, we continue to describe the bed lowering observed in the control experiment as subsidence.

Remarkably, the strong elevation-controlled signature of the control experiment is damped in the treatment. This could be because marsh sedimentation decreases the average delta slope by 50% in the marsh window (Sanks et al., 2022a), potentially reducing creep-based subsidence. Overall, it seems that marsh sedimentation decreases the slope of the delta, removing the near-shore creep failure mechanism, and adding a more spatially variable mechanism of marsh deposit compaction/consolidation.

Where can we expect to find this creep-style subsidence beyond our control experiment? It is likely to be found in other laboratory delta experiments with rising sea levels, and particularly those using fine-grained sediment. These deltas are constructed by flows that have a higher sediment to water ratio than field-scale systems, resulting in higher delta slopes and significantly altered morphodynamics (Sanks et al., 2023). Delta topset slopes tend to be multiple orders of magnitude lower than those observed in the control experiment, with similar slopes only widespread on the subaqueous foreset (Edmonds et al., 2011; Sanks et al., 2022a). While creep has been observed in coastal environments, we know of no field data that shows such tight elevation-control of subsidence rates.

By comparison, the treatment experiment produces subsidence that is larger in magnitude (Figure 2b) and more widespread than the control (Figure 3). Non-negligible subsidence rates extend from sea level to at least 25 mm RSL. Because the addition of marsh is the only change between experiments, this suggests that marsh sedimentation is influencing subsidence outside the active marsh window. This is unexpected because subsidence is shallow and weakly correlated with recent deposit thickness. This discrepancy can be explained by the fact that a large portion of subsidence in the treatment experiment is controlled by near surface compaction of clay layers, but a degree of marsh deposit compaction continues to occur for some time post-burial (Figure 7).

The behaviors described above establish that the experiments, and particularly the treatment experiment, have strong spatiotemporal variation in compactional subsidence rates. This is despite the fact that local average subsidence rates across the entire treatment experiment are controlled by the overall fraction of marsh in the subsurface (Figure 6). Therefore, the hot spots of above-average subsidence found at one time step do not predict continued above-average subsidence at the 2 hour timescale (Figure 5). Similar subsidence hot spots have been found on the Mississippi (Jankowski et al., 2017; Karengar et al., 2015; Morton et al., 2003), Ganges-Brahmaputra (Higgins et al., 2014), and Po (Teatini et al., 2011) deltas. While groundwater pumping and land use can cause persistent subsidence hotspots (Jones et al., 2016), our results show that there may be significant natural temporal variability in compactional subsidence as well.

Recent research comparing bulk densities of Mississippi River Delta sediments over a wide range of lithologies and burial depths shows that most subsidence occurs due to compaction within the upper 10 m of sediment (Jankowski et al., 2017; Keogh, 2020; Zumberge et al., 2022), or even deposits less than 100 years old and well within a meter of the surface (Keogh, 2020). Similarly, compactional subsidence rates in the Ganges-Brahmaputra Delta decay exponentially with depth, with the majority occurring within approximately 1–2 channel depths, or about 25–50 m (Steckler et al., 2022). These findings match well with the exponential decay in subsidence rates with depth found in the treatment experiment (Figure 7). In both field and experimental settings, at least half of the total subsidence is occurring in recent marsh deposits shallower than about one channel depth. This near surface bed lowering is continuously replenished by new marsh accretion and therefore does not contribute much

to the long-term generation of accommodation space, as  $\sigma_s$  accounts for only about one quarter of  $RSLR_b$  below a channel depth (Figure 7b). Field (van Asselen, 2011) and modeling (Kim et al., 2010; Liang et al., 2016; Moodie & Passalacqua, 2021; Xotta et al., 2022) studies have repeatedly shown the potential influence of subsidence on surface morphology and kinematics by causing differential compaction and steering channels. However, the treatment experiment, along with notable examples from field-scale deltas (e.g., Keogh, 2020; Steckler et al., 2022), suggest that compactional subsidence is often too shallow to significantly impact surface processes in this way.

The treatment experiment represents a first pass at understanding coupling between river deltas and marshes. Future work will link dynamic subsidence rates to marsh platform stability, delta top kinematics, and stratigraphic stacking patterns of coal seams. Continued field and numerical modeling efforts will extend our ability to reliably predict subsidence rates in low elevation coastal zones past the decadal timescale, where they likely remain spatially and temporally variable even under natural conditions.

## 5. Conclusion

This paper represents the first detailed analysis of subsidence within a compacting experimental delta deposit. Subsidence rates across the delta top of experiments both treated and untreated with a marsh proxy are non-negligible. The control experiment experienced rapid bed lowering slightly landward of the coast, likely triggered by localized soil creep. Nevertheless, the marsh proxy treatment produced subsidence rates that were on average twice as large as in the control experiment. Subsidence patterns in the treatment experiment more closely resemble field scale measurements from some global deltas in their spatial and temporal heterogeneity over short timescales, contribution to total RSLR, and mechanism of shallow compaction. The compaction of deeply buried marsh deposits appears to be relatively less important than surficial compaction in the experimental setting. These experimental results give valuable predictions of shallow subsidence in space and time that can inform management, modeling, and sustainability initiatives for global deltas.

## Conflict of Interest

The authors declare no conflicts of interest relevant to this study.

## Data Availability Statement

The data needed to reproduce the results in this study can be found at: [https://figshare.com/articles/dataset/Subsidence\\_Experimental\\_Deltas/21197728](https://figshare.com/articles/dataset/Subsidence_Experimental_Deltas/21197728), or (Zapp, 2022). These data can then be used to reproduce the results of this study when processed with the software located at: [https://github.com/SamZapp/Subsidence\\_Experimental\\_Deltas](https://github.com/SamZapp/Subsidence_Experimental_Deltas) or (Zapp, 2022). Raw experimental data is also available for TDB-18-1 (Straub & Dutt, 2022), and TDWB-19-2 (Sanks et al., 2022b).

## Acknowledgments

The project was funded by an NSF grant (co PIs Kyle Straub; NSF EAR-1848994 that funded Kyle Straub and Jose Silvestre's time plus much of the experimental costs and John Shaw; NSF EAR-1848993 that funded John Shaw and Samuel Zapp's time plus some experimental costs).

## References

- Bruno, L., Amorosi, A., Severi, P., & Costagli, B. (2017). Late Quaternary aggradation rates and stratigraphic architecture of the southern Po Plain, Italy. *Basin Research*, 29(2), 234–248. <https://doi.org/10.1111/bre.12174>
- Byrnes, M. R., Britch, L. D., Berlinghoff, J. L., Johnson, R., & Khalil, S. (2019). Recent subsidence rates for Barataria Bay, Louisiana. *Geo-Marine Letters*, 39(4), 265–278. <https://doi.org/10.1007/s00367-019-00573-3>
- Cahoon, D. R., Lynch, J. C., Roman, C. T., Schmit, J. P., & Skidgs, D. E. (2019). Evaluating the relationship among wetland vertical development, elevation capital, sea-level rise, and tidal marsh sustainability. *Estuaries and Coasts*, 42(1), 1–15. <https://doi.org/10.1007/s12237-018-0448-x>
- Chamberlain, E. L., Shen, Z., Kim, W., McKinley, S., Anderson, S., & Törnqvist, T. E. (2021). Does load-induced shallow subsidence inhibit delta growth? *Journal of Geophysical Research: Earth Surface*, 126(11), e2021JF006153. <https://doi.org/10.1029/2021JF006153>
- Chambers, L. G., Steinmuller, H. E., & Breithaupt, J. L. (2019). Toward a mechanistic understanding of “peat collapse” and its potential contribution to coastal wetland loss. *Ecology*, 100(7), e02720. <https://doi.org/10.1002/ecs.2720>
- Chang, C., Mallman, E., & Zoback, M. (2014). Time-dependent subsidence associated with drainage induced compaction in Gulf of Mexico shales bounding a severely depleted gas reservoir. *AAPG Bulletin*, 98(6), 1145–1159. <https://doi.org/10.1306/11111313009>
- Couvillion, B. R., Beck, H., Schoolmaster, D., & Fischer, M. (2017). *Land area change in coastal Louisiana (1932 to 2016) (USGS Numbered Series No. 3381) (IP-085820)*. U.S. Geological Survey. Retrieved from <http://pubs.er.usgs.gov/publication/sim3381>
- Dokka, R. K. (2006). Modern-day tectonic subsidence in coastal Louisiana. *Geology*, 34(4), 281–284. <https://doi.org/10.1130/G22264.1>
- Edmonds, D. A., Shaw, J. B., & Mohrig, D. (2011). Topset-dominated deltas: A new model for river delta stratigraphy. *Geology*, 39(12), 1175–1178. <https://doi.org/10.1130/G32358.1>
- Engle, V. D. (2011). Estimating the provision of ecosystem services by Gulf of Mexico coastal wetlands. *Wetlands*, 31(1), 179–193. <https://doi.org/10.1007/s13157-010-0132-9>
- Erban, L. E., Gorelick, S. M., & Zebker, H. A. (2014). Groundwater extraction, land subsidence, and sea-level rise in the Mekong Delta, Vietnam. *Environmental Research Letters*, 9(8), 084010. <https://doi.org/10.1088/1748-9326/9/8/084010>



- Higgins, S. A., Overeem, I., Steckler, M. S., Syvitski, J. P. M., Seeber, L., & Akhter, S. H. (2014). InSAR measurements of compaction and subsidence in the Ganges-Brahmaputra Delta, Bangladesh. *Journal of Geophysical Research: Earth Surface*, *119*(8), 1768–1781. <https://doi.org/10.1002/2014JF003117>
- Hoyal, D. C. J. D., & Sheets, B. A. (2009). Morphodynamic evolution of experimental cohesive deltas. *Journal of Geophysical Research*, *114*(F2), F02009. <https://doi.org/10.1029/2007JF000882>
- Ishii, Y., Tamura, T., & Ben, B. (2021). Holocene sedimentary evolution of the Mekong River floodplain, Cambodia. *Quaternary Science Reviews*, *253*, 106767. <https://doi.org/10.1016/j.quascirev.2020.106767>
- Jankowski, K. L., Tornqvist, T. E., & Fernandes, A. M. (2017). Vulnerability of Louisiana's coastal wetlands to present-day rates of relative sea-level rise. *Nature Communications*, *8*, 1–7. <https://doi.org/10.1038/ncomms14792>
- Jones, C. E., An, K., Blom, R. G., Kent, J. D., Ivins, E. R., & Bekaert, D. (2016). Anthropogenic and geologic influences on subsidence in the vicinity of New Orleans, Louisiana. *Journal of Geophysical Research: Solid Earth*, *121*(5), 3867–3887. <https://doi.org/10.1002/2015JB012636>
- Karengar, M. A., Dixon, T. H., & Malservisi, R. (2015). A three-dimensional surface velocity field for the Mississippi Delta: Implications for coastal restoration and flood potential. *Geology*. <https://doi.org/10.1130/G36598.1>
- Keogh, M. E. (2020). *Accretion, compaction, and restoration: Sediment dynamics and relative sea-level rise in coastal wetlands (unpublished PhD dissertation)*. Tulane University.
- Keucher, G. (1994). *Geologic framework and consolidation settlement potential of the Lafourche delta, Topstratum valley fill; Implications for wetland loss in Terrebonne and Lafourche Parishes, Louisiana (PhD)*. Louisiana State.
- Kim, W., Sheets, B. A., & Paola, C. (2010). Steering of experimental channels by lateral basin tilting. *Basin Research*, *22*(3), 286–301. <https://doi.org/10.1111/j.1365-2117.2009.00419.x>
- Kirwan, M. L., & Guntenspergen, G. R. (2010). Influence of tidal range on the stability of coastal marshland. *Journal of Geophysical Research*, *115*(F2), F02009. <https://doi.org/10.1029/2009JF001400>
- Kooi, H., & de Vries, J. (1998). Land subsidence and hydrodynamic compaction of sedimentary basins. *Hydrology and Earth System Sciences*, *2*(2/3), 159–171. <https://doi.org/10.5194/hess-2-159-1998>
- Liang, M., Kim, W., & Passacqua, P. (2016). How much subsidence is enough to change the morphology of river deltas? *Geophysical Research Letters*, *43*(19), 10266. <https://doi.org/10.1002/2016GL070519>
- Mariotti, G. (2020). Beyond marsh drowning: The many faces of marsh loss (and gain). *Advances in Water Resources*, *144*, 103710. <https://doi.org/10.1016/j.advwatres.2020.103710>
- Meckel, T., ten Brink, U., & Williams, S. (2006). Current subsidence rates due to compaction of Holocene sediments in southern Louisiana. *Geophysical Research Letters*, *33*(11), L11403. <https://doi.org/10.1029/2006GL026300>
- Mesri, G., Stark, T., Ajlouni, M., & Chen, M. (1997). Secondary compression of peat with or without surcharging. *Journal of Geotechnical and Geoenvironmental Engineering*, *123*(5), 411–421. [https://doi.org/10.1061/\(asce\)1090-0241\(1997\)123:5\(411\)](https://doi.org/10.1061/(asce)1090-0241(1997)123:5(411))
- Minderhoud, P. S. J., Erkens, G., Pham, V. H., Bui, V. T., Erban, L., Kooi, H., & Stouthamer, E. (2017). Impacts of 25 years of groundwater extraction on subsidence in the Mekong delta, Vietnam. *Environmental Research Letters*, *12*(6), 064006. <https://doi.org/10.1088/1748-9326/aa7146>
- Moodie, A. J., & Passalacqua, P. (2021). When does faulting-induced subsidence drive distributary network reorganization? *Geophysical Research Letters*, *48*(22), e2021GL095053. <https://doi.org/10.1029/2021GL095053>
- Morris, J. T., Sundareshwar, P., Nietch, C. T., Kjerfve, B., & Cahoon, D. (2002). Responses of coastal wetlands to rising sea level. *Ecology*, *83*(10), 2869–2877. [https://doi.org/10.1890/0012-9658\(2002\)083\[2869:ROCWTR\]2.0.CO;2](https://doi.org/10.1890/0012-9658(2002)083[2869:ROCWTR]2.0.CO;2)
- Morton, R., Bernier, J., & Barras, J. (2006). Evidence of regional subsidence and associated interior wetland loss induced by hydrocarbon production, Gulf Coast region, USA. *Environmental Geology*, *50*(2), 14–274. <https://doi.org/10.1007/s00254-006-0207-3>
- Morton, R., Tiling, G., & Ferina, N. F. (2003). Causes of hot-spot wetland loss in the Mississippi delta plain. *Environmental Geosciences*, *10*(2), 71–80. <https://doi.org/10.1306/eg.04040302007>
- Nienhuis, J. H., Törnqvist, T. E., Jankowski, K. L., Fernandes, A. M., & Keogh, M. E. (2017). A new subsidence map for coastal Louisiana. *Geological Society of America Today*, 60–61. <https://doi.org/10.1130/GSATG337GW.1>
- Paola, C., Straub, K. M., Mohrig, D., & Reinhardt, L. (2009). The “unreasonable effectiveness” of stratigraphic and geomorphic experiments. *Earth-Science Reviews*, *97*(1–4), 1–43. <https://doi.org/10.1016/j.earscirev.2009.05.003>
- Sanks, K. M., Shaw, J. B., & Naithani, K. (2020). Field-based estimate of the sediment deficit in coastal Louisiana. *Journal of Geophysical Research: Earth Surface*, *125*(8), e2019JF005389. <https://doi.org/10.1029/2019JF005389>
- Sanks, K. M., Shaw, J., Zapp, S. M., Silvestre, J., Dutt, R., & Straub, K. M. (2023). Marsh induced backwater: The influence of non-fluvial sedimentation on a delta's channel morphology and kinematics. In *EGU sphere* (pp. 1–36). <https://doi.org/10.5194/egusphere-2023-545>
- Sanks, K. M., Zapp, S. M., Silvestre, J., Shaw, J. B., Dutt, R., & Straub, K. M. (2022a). Marsh sedimentation controls delta top morphology, slope, and mass balance. *Geophysical Research Letters*, *49*(12), e2022GL098513. <https://doi.org/10.1029/2022GL098513>
- Sanks, K. M., Zapp, S. M., Silvestre, J., Shaw, J. B., & Straub, K. M. (2022b). *TDWB-19-2-surface-processes*. SEAD. <https://doi.org/10.26009/sOUQYZ0M>
- Shirzaei, M., Freymueller, J., Törnqvist, T. E., Galloway, D. L., Dura, T., & Minderhoud, P. S. J. (2021). Measuring, modelling and projecting coastal land subsidence. *Nature Reviews Earth & Environment*, *2*(1), 40–58. <https://doi.org/10.1038/s43017-020-00115-x>
- Steckler, M. S., Oryan, B., Wilson, C. A., Grall, C., Nooner, S. L., Mondal, D. R., et al. (2022). Synthesis of the distribution of subsidence of the lower Ganges-Brahmaputra Delta, Bangladesh. *Earth-Science Reviews*, *224*, 103887. <https://doi.org/10.1016/j.earscirev.2021.103887>
- Straub, K. M., & Dutt, R. (2022). *TDWB-18*. SEAD. <https://doi.org/10.26009/sOG2SM3L>
- Straub, K. M., Li, Q., & Benson, W. M. (2015). Influence of sediment cohesion on deltaic shoreline dynamics and bulk sediment retention: A laboratory study. *Geophysical Research Letters*, *42*(22), 9808–9815. <https://doi.org/10.1002/2015GL066131>
- Syvitski, J., Kettner, A., Overeem, I., Hutton, E., Hannon, M., Brackenkridge, G. R., et al. (2009). Sinking deltas due to human activities. *Nature Geoscience*, *2*(10), 681–686. <https://doi.org/10.1038/ngeo629>
- Teatini, P., Tosi, L., & Strozzi, T. (2011). Quantitative evidence that compaction of Holocene sediments drives the present land subsidence of the Po Delta, Italy. *Journal of Geophysical Research*, *116*(B8), B08407. <https://doi.org/10.1029/2010JB008122>
- Törnqvist, T. E., Wallace, D. J., Storms, J. E. A., Wallinga, J., van Dam, R. L., Blaauw, M., et al. (2008). Mississippi Delta subsidence primarily caused by compaction of Holocene strata. *Nature Geoscience*, *1*(3), 173–176. <https://doi.org/10.1038/ngeo129>
- Vallejo, L. E. (1980). Mechanics of mudflow mobilization in low-angled clay slopes. *Engineering Geology*, *16*(1), 63–70. [https://doi.org/10.1016/0013-7952\(80\)90007-1](https://doi.org/10.1016/0013-7952(80)90007-1)
- van Asselen, S. (2011). The contribution of peat compaction to total basin subsidence: Implications for the provision of accommodation space in organic-rich deltas. *Basin Research*, *23*(2), 239–255. <https://doi.org/10.1111/j.1365-2117.2010.00482.x>
- Xotta, R., Zoccarato, C., Minderhoud, P. S. J., & Teatini, P. (2022). Modeling the role of compaction in the three-dimensional evolution of depositional environments. *Journal of Geophysical Research: Earth Surface*, *127*(9), e2022JF006590. <https://doi.org/10.1029/2022JF006590>

- Yuill, B., Lavoie, D., & Reed, D. (2009). Understanding subsidence processes in coastal Louisiana. *Journal of Coastal Research*, 10054(54), 23–36. <https://doi.org/10.2112/si54-012.1>
- Zapp, S. M. (2022). SamZapp/Subsidence\_experimental\_deltas:v1. *Zenodo*. <https://doi.org/10.5281/zenodo.7183295>
- Zumberge, M. A., Xie, S., Wyatt, F. K., Steckler, M. S., Li, G., Hatfield, W., et al. (2022). Novel integration of Geodetic and geologic methods for high-resolution Monitoring of subsidence in the Mississippi delta. *Journal of Geophysical Research: Earth Surface*, 127(9), e2022JF006718. <https://doi.org/10.1029/2022JF006718>